Prediction of Turbulent Combustion Flowfields Behind a Backward-Facing Step

Fang H. Tsau* and Warren C. Strahle†
Georgia Institute of Technology, Atlanta, Georgia 30332

Turbulent combustion flowfields behind a backward-facing step are examined by using different boundary conditions and various computational assumptions. The effect of combustion on the flow is also studied. Hydrogen and methane are the two gaseous fuels chosen for this investigation. Both a conventional law of the wall method and a recently developed low Reynolds number model are tested. Two types of statistical models are employed in the combustion simulations to take into account species fluctuations. The results are primarily fourfold: 1) The fluctuation of the fuel mass fraction is insignificant for the Reynolds number examined in this paper; 2) different statistical models produce almost identical results; 3) the law of the wall model predicts a shorter reattachment length than the low Reynolds number model does; and 4) the effect of combustion is to shorten the reattachment length of the flowfield, and the reattachment length is more a function of the amount of heat input to the system than a function of the type of fuel or a function of the injection rate in a reactive flow system.

Nomenclature

f = statistical mean
g = Favre covariance of the mixture fraction
k = specific turbulence kinetic energy, m^2/s^2
m = $(\rho V)_0/(\tau_0\rho_0)^{1/2}$
P = probability density function
p = pressure, N/m^2
R_s = residual
S_ϕ = source term in an equation
T = temperature, K
U = streamwise velocity, m/s
U_i = Cartesian velocity component, m/s
u_i'' = Favre fluctuation of velocity component U_i, m/s
V = transverse velocity, m/s
x_i = Cartesian coordinate, m
x = streamwise coordinate, m
y = transverse coordinate, m
ϵ = turbulence dissipation rate, m^2/s^3
η = mixture fraction
η'' = Favre fluctuation of mixture fraction
κ = von Kármán constant
μ = laminar viscosity, kg/m · s
μ_T = eddy viscosity, kg/m · s
μ_{eff} = $\mu + \mu_T$
ν = kinematic viscosity, m^2/s
ρ = density, kg/m^3
σ = statistical variance
τ = stress, $kg/m \cdot s^2$
ϕ = any dependent variable

Subscripts

l = quantities inside the viscous sublayer
v = quantities at the edge of the viscous sublayer
0 = wall values
1 = first grid point outside the viscous sublayer or off the wall

Superscripts

$+$ = characteristic quantities in the near wall region
$-$ = time-averaged quantities
$\sim$ = Favre-averaged quantities

Received Dec. 24, 1987; presented as Paper 88-0340 at the AIAA 26th Aerospace Sciences Meeting, Reno, NV, Jan. 11-14, 1988; revision received July 11, 1989.

*Graduate Research Assistant, School of Aerospace Engineering.
†Regent's Professor, School of Aerospace Engineering. Fellow AIAA.

Introduction

INCREASED interest in the application of ramjet propulsion systems has led to a large amount of research in dump-type combustor flow systems. Early work of Jones and Launder,[1] Launder et al.,[2] Rodi,[3] Launder and Spalding,[4] and their successors has been used by recent researchers in modeling isothermal turbulent flows in such dump combustor configurations. Several approximations necessarily arise in the analytical treatment of these flowfields. For one, the application of the so-called wall-function approach in wall-bounded flows has allowed researchers to relate surface boundary conditions to points in the flowfield where the Reynolds number is sufficiently high for viscous effects to be negligible. It is, however, not too difficult to imagine there are instances in which this approach may not be valid, especially considering the assumptions incorporated in the model itself. Also, its accuracy in a wall-bounded, reactive flow system still remains to be determined.

To generalize existing turbulence modeling techniques to resolve the viscous sublayer whenever it is necessary, researchers started looking into the possibility of adapting the high Reynolds number models to account for the viscous effects. Theoretically, one may just pick up every term that had been omitted in the development of the high Reynolds number model, mathematically model each one of them, and include all of them in the modeled governing equations. However, no models can be put forth before the physics in the near-wall region are further understood. Alternatively, the so-called damping terms may be added to the high Reynolds number equations to balance the equations in the low Reynolds number region of a flow. For both of the above approaches, the entire set of turbulence model constants may have to be replaced by functions of Reynolds number and/or reoptimized so that the viscous effects can be included. Moreover, these numerical damping functions were not rigorously derived, and the functions lack physical bases. Such an alternative approach has been taken by Chieng and Launder,[5] Lam and Bremhorst,[6] Chien,[7] and others. A third approach is to take the high Reynolds number model as it is and curve fit the low

Reynolds number region using evidence from the still limited experimental information directly. This approach was first taken by Gorski.[8] The ultimate goal of modeling the turbulent flows is, of course, to have a model which is applicable to a wide class of problems and able to produce results in good agreement with known experimental data. The third approach by Gorski fulfills the above general requirements and has sounder physical bases. It is therefore adopted in this research.

It was not until about a decade ago that researchers started trying to include chemical reactions in their fluid dynamic calculations. Bilger,[9] Kent and Bilger,[10] Janicka and Kollmann,[11] and Spalding[12] are, for example, among those early workers. Accurate chemical kinetic data is, of course, essential, but two of the most difficult aspects in developing a combustion model are first, understanding of how the combustion processes interact with the fluid problem and, second, where and how the model can be compromised with reality so that it is tractable mathematically. Furthermore, the theoretical development also suffers from a lack of experimental results, which are essential for verifying and developing a computational model. A full account of interaction between chemical kinetics and fluid dynamics is still difficult nowadays as far as numerical calculation is concerned. Simplified models were developed by Bilger, Spalding, and Janicka and Kollmann as mentioned before, and recent developments and concerns were brought up, for example, by Peters and Kee,[13] Drummond,[14] Rogers and Chinitz,[15] and Ballal and Chen.[16] The idea of Spalding[17] is employed as the fundamental framework of the combustion models discussed in this paper. This research compares results from a high Reynolds number model and a low Reynolds number model, and the effect of species fluctuations is examined for a current experimental configuration which models a dump-type combustor.

Theoretical Development

An idealized ramjet combustion chamber is depicted in Fig. 1, where the region bounded by two arrows at the bottom is the fuel port through which pure hydrogen or methane is injected into the chamber. This configuration models an experimental apparatus of the combustion laboratory at Georgia Institute of Technology.[18] The turbulent flowfield is assumed to be stationary and adiabatic. The chemical reaction rates are assumed to be infinitely fast so that the mixture is in chemical equilibrium everywhere inside the chamber. This implies that reversible multistep reactions are considered and that chemical reactions are not limited in a thin flame sheet. The equilibrium assumption is very suitable for systems consisting of highly energetic chemical elements, such as hydrogen and oxygen, and is expected to be good around the stoichiometric line and poorer away from it. The Favre-averaging technique (density-weighted averaging) is adopted in the formulation due to expected large density gradient present in the flow. Bilger[9] and Jones[19] have argued that the Favre-averaging technique is superior to the conventional Reynolds-averaging technique from both physical and numerical points of view for variable-density flows. A Favre-averaging quantity $\tilde{Q}$ of Q is defined by

$$\tilde{Q} = \overline{\rho Q}/\bar{\rho} \tag{1}$$

or

$$\tilde{Q} = \int_Q Q\tilde{P}\,dQ \tag{2}$$

Bearing the above relations in mind, one may obtain the following averaged Navier-Stokes equations:

$$\frac{\partial}{\partial x_i}(\bar{\rho}\tilde{U}_i) = 0 \tag{3}$$

$$\frac{\partial}{\partial x_j}(\bar{\rho}\tilde{U}_i\tilde{U}_j) = -\frac{\partial \bar{p}}{\partial x_i} + \frac{\partial}{\partial x_j}\left[\mu_{\text{eff}}\left(\frac{\partial \tilde{U}_j}{\partial x_i} + \frac{\partial \tilde{U}_i}{\partial x_j}\right)\right] - \frac{2}{3}\delta_{ij}\frac{\partial}{\partial x_j}\left(\bar{\rho}\tilde{k} + \mu_{\text{eff}}\frac{\partial \tilde{U}_n}{\partial x_n}\right) \tag{4}$$

in which the Favre stress term $\overline{\rho u_i'' u_j''}$ is modeled as in Jones[19]

$$\overline{\rho u_i'' u_j''} = \frac{2}{3}\delta_{ij}\left(\bar{\rho}\tilde{k} + \mu_T\frac{\partial \tilde{U}_n}{\partial x_n}\right) - \mu_T\left(\frac{\partial \tilde{U}_i}{\partial x_j} + \frac{\partial \tilde{U}_j}{\partial x_i}\right)$$

and all of the correlation terms involving laminar viscosity are neglected in comparison with both the Favre stress term and the mean stress term. This incomplete modeling of the momentum equations is partly due to a lack of available models at hand.[19]

This research uses the well-known, two-equation k-ϵ model to close the fluid dynamic problem. The k equation in this case is

$$\frac{\partial}{\partial x_j}(\bar{\rho}\tilde{U}_j\tilde{k}) = \frac{\partial}{\partial x_j}\left[\left(\bar{\mu} + \frac{\mu_T}{\sigma k}\right)\frac{\partial \tilde{k}}{\partial x_j}\right] - \bar{\rho}\tilde{\epsilon} + \left(1 - \frac{2}{3}\alpha_1\right)\left(-\overline{\rho u_i'' u_j''}\frac{\partial \tilde{U}_j}{\partial x_i}\right) + \frac{1}{3}\alpha_2\overline{\rho u_n''^2}\frac{\partial \tilde{U}_i}{\partial x_i} \tag{5}$$

in which the velocity-pressure gradient term $\overline{u_j''(\partial p)/(\partial x_j)}$ is modeled as in Strahle[20]

$$\overline{u_j''\frac{\partial p}{\partial x_j}} = -\frac{2}{3}\alpha_1\overline{\rho u_i'' u_j''}\frac{\partial \tilde{U}_j}{\partial x_i} - \frac{1}{3}\alpha_2\overline{\rho u_n''^2}\frac{\partial \tilde{U}_i}{\partial x_i}$$

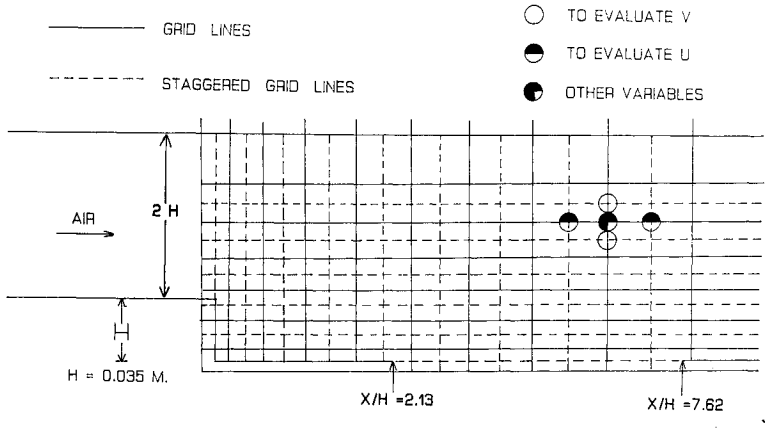

Fig. 1 Grid setup and some characteristic dimensions.

The ϵ equation is directly taken over from the constant density version and interpreted in a Favre sense

$$\frac{\partial}{\partial x_j}(\bar{\rho}\tilde{U}_j\tilde{\epsilon}) = \frac{\partial}{\partial x_j}\left[\left(\mu + \frac{\mu_T}{\sigma\epsilon}\right)\frac{\partial\tilde{\epsilon}}{\partial x_j}\right] - C_2\bar{\rho}\frac{\tilde{\epsilon}^2}{\tilde{k}} + C_1\left(-\overline{\rho u_i'' u_j''}\frac{\partial\tilde{U}_i}{\partial x_j}\right)\frac{\tilde{\epsilon}}{\tilde{k}} \quad (6)$$

This direct transformation of the dissipation rate equation is due to a lack of information on the dissipation rate, especially for a reactive flow system. In the case of combustion, two additional variables are introduced into the formulation of the problem, namely the mixture fraction η (a conserved scalar) and its covariance $\tilde{\eta}''^2$ (g). The mixture fraction may be physically interpreted as the mass fraction of material in the mixture, which originates from the fuel stream, with $(1-\eta)$ originating from the air (oxidizer) stream. In this regard, the system is mathematically modeled as a binary chemical system that has only one relevant molecular diffusivity. It can be shown, with the assumption of equal diffusivity for all the species, that all conserved scalars in a reactive flow system are linearly related. Furthermore, if one assumes the Lewis number to be unity and the Mach number of the flow to be small, the solutions to the energy equation and the species conservation equation are fully similar.[21] For this reason, only the equation of the mixture fraction is included here

$$\frac{\partial}{\partial x_j}(\bar{\rho}\tilde{U}_j\tilde{\eta}) = \frac{\partial}{\partial x_j}\left[\frac{(\mu+\mu_T)}{\sigma_\eta}\frac{\partial\tilde{\eta}}{\partial x_j}\right] \quad (7)$$

in which the turbulent Schmidt number is assumed to be 0.7, and a gradient diffusion model is employed to model the turbulent flux term $\overline{\rho u_j'' \eta}$. The equation for the covariance is taken over from Spalding[17] as

$$\frac{\partial}{\partial x_j}(\bar{\rho}\tilde{U}_j g) = \frac{\partial}{\partial x_j}\left[\frac{(\bar{\mu}+\mu_T)}{\sigma_g}\frac{\partial g}{\partial x_j}\right] + C_{g1}\mu_T\left(\frac{\partial\tilde{\eta}}{\partial x_j}\right)^2 - C_{g2}\frac{\bar{\rho}\tilde{\epsilon}}{\tilde{k}}g \quad (8)$$

Table 1 summarizes all relevant dependent variables and model constants associated with turbulence models.

Several cases are studied and summarized below.

1) For cold flow simulation without side-wall injection, Eqs. (3-6) are solved simultaneously with the divergence of the velocity vector being equal to zero, i.e.,

$$\frac{\partial\tilde{U}_i}{\partial x_i} = 0$$

2) For cold flow simulation with side-wall injection, Eqs. (3-7) are solved simultaneously with the assumption that density gradients are negligible inside the chamber. This is justified by the fact that the fuel injection rates are very small. Local density and laminar viscosity are uniquely determined by the local mixture fraction from the perfect gas law.

3) For combustion simulations neglecting species fluctuations, Eqs. (3-7) are solved simultaneously. Local density, temperature, and laminar viscosity are only functions of the mixture fraction. Fluid properties are obtained from a chemical equilibrium computer code by Gordon and McBride.[22] Both a law of the wall model and a low Reynolds number model are tested for this case.

4) For combustion simulations with species fluctuations taken into account, Eqs. (3-8) are solved simultaneously. Local density, temperature, and laminar viscosity are functions of mixture fraction and its covariance. Two types of probability density functions (PDFs) are presumed in this research. Tables of density, temperature, and laminar viscosity in terms of mixture fraction and its covariance are constructed by utilizing chemical equilibrium data and the assumed PDFs in order to facilitate calculations. Only the low Reynolds number model is explored for this case.

Table 1 Dependent variables and model constants

$\tilde{U}$	$\tilde{V}$	$\tilde{k}$	$\tilde{\epsilon}$	$\tilde{\eta}$	g
C_μ 0.09	C_μ 0.09	α_1 0.067	C_1 1.44	σ_η 0.7	C_{g1} 2.8
κ 0.42	κ 0.42	α_2 1.54	C_2 1.92		C_{g2} 2.0
		σ_k 1.0	σ_ϵ 1.3		σ_g 0.7

Model and Numerical Details

The law of the wall model relates surface boundary conditions to points in the flowfield where the Reynolds number is sufficiently high. In essence, this model assumes that at a point outside the viscous sublayer (usually it is the first grid node off the physical wall boundary in the high Reynolds number model calculation), the streamwise velocity component follows the logarithmic law of the wall and that the turbulence is in local equilibrium such that the production of turbulence energy equals its dissipation. If one neglects the pressure gradient effect and the streamwise convective and diffusive transport in addition to the above assumptions, the following near-wall model can be established[23]

$$U^+ = \frac{1}{\kappa}\ell n(Ey^+) + m\left[\frac{1}{2\kappa}\ell n(Ey^+)\right]^2 \quad (9)$$

$$\eta_0 = \frac{\eta_1 - 1}{[1+mU^+]^{\sigma\eta}} + 1 \quad (10)$$

$$\tau_1 = \frac{\bar{\rho}_1\tilde{U}_1 C_\mu^{1/4}\tilde{k}_1^{1/2}}{(1/\kappa)\ell n\,(Ey^+)} + \rho_1\tilde{U}_1 V_0 - V_0\frac{\bar{\rho}_1 C_\mu^{1/4}\tilde{k}_1^{1/2}}{4}\left[\frac{1}{\kappa}\ell n\,(Ey^+)\right] \quad (11)$$

in which E is an integration constant taking on the value 9.5[5] for a solid wall. For a permeable wall, E is evaluated according to the method developed in Ref. 23 and is usually less than 9.5. A corresponding V^+, τ_1 and η_0 with respect to the vertical step can be obtained by setting V_0 equal to zero and substituting x and V for y and U respectively in Eqs. (9-11).

Equations (5), (6), and (8) are only valid in a high Reynolds number region.[17,19] That is why the law of the wall model is necessary to bridge the gap between a wall boundary and the logarithmic region in early work. As the information inside the viscous sublayer becomes more available, it is tempting to try to resolve the flowfield completely. The main theme of the low Reynolds number model adopted in this paper is to numerically curvefit the region inside the viscous sublayer with known turbulence behavior while the region of sufficiently high Reynolds number (assumed to be 20 and above which corresponds to a characteristic length $y^+ \sim 12$ and above in this research) is still governed by Eqs. (4-8). Current experimental data shows that the turbulence kinetic energy is proportional to the square of the distance from the wall, and the dissipation rate is roughly constant inside the viscous sublayer. Gorski[8] made another curve fit for the eddy viscosity inside the viscous sublayer and found that the eddy viscosity is proportional to the cubic power of distance from the wall. The above observations can be mathematically expressed as

$$\tilde{k}_l = \tilde{k}_v\left(\frac{y_l}{y_v}\right)^2 \quad (12)$$

$$\tilde{\epsilon}_l = 2\nu\left(\frac{\partial\tilde{k}^{1/2}}{\partial y}\right)^2 = \frac{2\nu\tilde{k}_v}{y_v^2} \quad (13)$$

and

$$\mu_{T_l} = \mu_{T_v}\left(\frac{y_l}{y_v}\right)^3 \quad (14)$$

and the shear stress on the wall is simply, by a forward

differencing scheme,

$$\tau_0 = \mu_0 \frac{\tilde{U}_1}{y_1} \tag{15}$$

where

$$\tilde{k}_v = \frac{\tau_0}{\rho_0 \sqrt{C_\mu}}$$

is based on local equilibrium turbulence assumption. The same treatment can be applied along the vertical step. In fact, Patel et al.[24] had shown that, by using Launder's description of the variation of the instantaneous velocity components inside a viscous sublayer, Eqs. (12–14) are indeed good approximations in the near-wall viscous region. There is no available theoretical model or experimental evidence to demonstrate how g varies inside a viscous sublayer so far. The authors propose the following relationship in light of the source terms of Eq. (8)

$$g_l = g_v \left(\frac{y_l}{y_v}\right)^3 \tag{16}$$

which might be the maximum possible covariance as far as the exponent is concerned. One advantage of employing the above low Reynolds number model is that one may have as many numerical grid points in the near-wall region as possible without encountering a numerical stiffness problem arising from using other low Reynolds number models.[1,7]

To solve the system of equations simultaneously, a hybrid discretization scheme[25] is employed. A general discretized equation can be written as

$$A_P \phi_P = A_N \phi_N + A_S \phi_S + A_E \phi_E + A_W \phi_W + S\phi \tag{17}$$

where P is the point in question and E, W, S, and N are its surrounding neighbors with respect to the same dependent variables concerned. The A are coefficients resulting from the hybrid discretization scheme. A solution procedure named SIMPLE,[25] which uses a tridiagonal matrix solver to solve the discretized equations of the entire flowfield, is chosen to accomplish the iterative procedures. A basic grid system, which has 31 grid lines in the streamwise direction with an expansion ratio of 1.15 and 41 grid lines with constant spacing in the transverse direction, is adopted from Richardson.[23] When the low Reynolds number model is used, 20 more grid lines are buried into the region between the bottom wall boundary (the fuel side) and the first transverse grid line of the basic grid system. A 31 by 37 grid system is employed for combustion simulation using the law of the wall model. The expansion ratio in the streamwise direction for the 31 by 37 and 31 by 61 grid systems is 1.07.

The boundary condition at the outlet (which is 32 step heights downstream from the inlet) of the combustion chamber is that the gradients are zero for all of the dependent variables. Experimental measurements from our laboratory are taken to be the boundary conditions at the inlet. Pertinent shear forces from Eqs. (11) or (15) are used as boundary conditions for momentum equations on wall boundaries. For the simulation employing the high Reynolds number model, Eq. (5) is solved at the first grid off the wall by using an averaged $\tilde{\epsilon}$ and production term estimated from Eqs. (9) and (11) to accurately represent the wall region. The dissipation rate is simply set to be $C_\mu^{3/4} k_1^{3/2}/(\kappa y_1)$. For simulations using the low Reynolds number model, the first grid point outside the viscous sublayer is determined frist, and the setup of the governing equations at this grid point proceeds in exactly the same way as in the high Reynolds number model. The covariance of the mixture fraction will be set equal to $C_{g1} \tilde{k}_1 \mu_T (\partial\tilde{\eta}/\partial x_j)^2/(C_{g2}\tilde{\rho}\tilde{\epsilon})$ if it solved. Linear extrapolations can be applied to estimate $\tilde{k}_v$ and g_v and values of $\tilde{k}$, $\tilde{\epsilon}$, and g inside the viscous sublayer can then be found from Eqs. (12), (13), and (16) respectively. The boundary conditions of the conserved scalar $\tilde{\eta}$ are the same regardless of what model is employed, namely the normal gradient being zero at the solid wall boundary (in fact the total flux is zero) and the total flux (convection plus diffusion) at the porous wall boundary equal to the preset influx of fuel in our experiments.

As was mentioned before, two different kinds of PDFs are incorporated in the combustion model for reactive flow simulations with species fluctuations taken into account. The PDFs are depicted in Figs. 2 and 3. One should notice that the statistical mean and variance need not be the same as the calculated mean mixture fraction and the square root of the covariance because of the truncations on both ends of the regular Gaussian PDF. The truncations are necessary to exclude unrealistic mixture fractions inherent in the regular Gaussian distribution. The following relations set up the link between the mathematical models and the calculated mixture fraction and its covariance[26]

$$\tilde{\eta} = \int_0^1 \eta \tilde{P}_N \, d\eta = \frac{1}{B} \int_0^1 \eta \tilde{P}_0 \, d\eta \tag{18a}$$

$$g = \int_0^1 (\eta - \tilde{\eta})^2 \tilde{P}_N \, d\eta = \frac{1}{B} \int_0^1 \eta^2 \tilde{P}_0 \, d\eta - \tilde{\eta}^2 \tag{18b}$$

$$\tilde{\eta} = \int_0^1 \eta \tilde{P}_C \, d\eta = \int_1^\infty \tilde{P}_0 \, d\eta + \int_0^1 \eta \tilde{P}_0 \, d\eta \tag{18c}$$

$$g = \int_0^1 (\eta - \tilde{\eta})^2 \tilde{P}_C \, d\eta = \int_1^\infty \tilde{P}_0 \, d\eta + \int_0^1 \eta^2 \tilde{P}_0 \, d\eta - \tilde{\eta}^2 \tag{19}$$

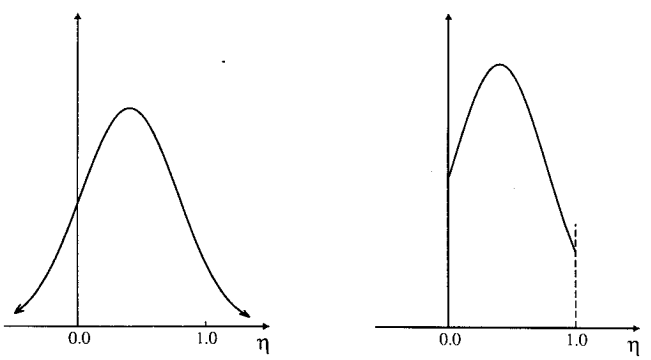

Fig. 2 Gaussian and normalized-Gaussian PDFs.

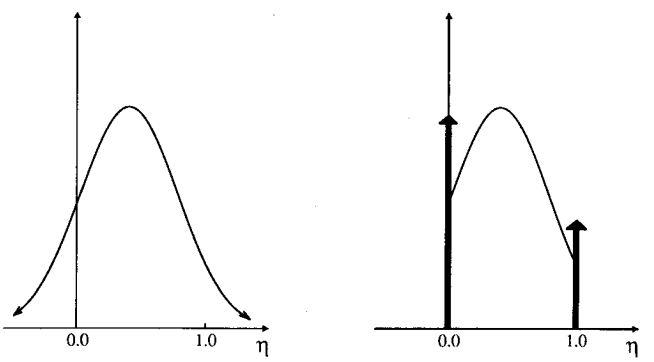

Fig. 3 Gaussian and clipped-Gaussian PDFs.

where

$$\tilde{P}_0 = \exp\left[-\frac{1}{2}\left(\frac{\eta - f}{\sigma}\right)^2\right] \Big/ (\sigma\sqrt{2\pi})$$

$\tilde{P}_N = \tilde{P}_0/B$, normalized-Gaussian PDF

$$\tilde{P}_C = \tilde{P}_0 + \delta(0)\int_{-\infty}^{0} \tilde{P}_0 d\eta + \delta(1)\int_{1}^{\infty} \tilde{P}_0 d\eta, \text{ clipped-Gaussian PDF}$$

$$B = \int_0^1 \tilde{P}_0 d\eta$$

Tables of density, temperature, and laminar viscosity in terms of $\tilde{\eta}$ and $\tilde{\eta}''^2$ are constructed, and two-dimensional searching and interpolating subroutines are employed to obtain various fluid properties for a given pair of $\tilde{\eta}$, g from the solutions of the corresponding conservation equations.

A residual of an algebraic equation like Eq. (17) can be defined in the following way

$$R_s = |A_P\phi_P - A_N\phi_N - A_S\phi_S - A_E\phi_E - A_W\phi_W - S\phi| \quad (20)$$

which is a measure of the satisfaction of the original differential equation at one particular grid point. Hence, the result of summing up all R_s through the entire calculation domain is a measure of the satisfaction of the original differential equation for the entire flowfield considered. The overall residuals of the momentum equations are normalized by the inlet momentum flux, and the overall residuals of the species conservation equation and the covariance equation are normalized by the total mass flux of the combustor. The iterative procedure in this research carries on until the overall residual of the continuity equation (the mass imbalance) is less than 1% of the mass flow rate at the exit of the combustor. The situation roughly corresponds to an overall residual of 1.0E-03 for the U-momentum equation, 1.0E-04 for the V-momentum equation, 1.0E-06 for the species conservation equation, and 1.0E-05 for the covariance equation, respectively. The solutions obtained for various cases are grid independent with respect to the theoretical framework (i.e., the high Reynolds number model or the low Reynolds number model) of each simulation.

Results and Discussion

Before combustion simulations were conducted, the low Reynolds number code was validated first by doing a cold flow, no injection simulation. Figure 4 shows the development of the normalized turbulence kinetic energy in the streamwise direction. The results are almost identical to the numerical results of Richardson,[23] which were verified by Richardson et al.[18] and de Groot.[27] The reattachment lengths quoted in column 1 of Table 2 are also from Ref. 23. The fact that the primary reattachment lengths are about the same from both codes indicates that the high Reynolds number model is indeed a good approximation in isothermal flow without side-wall injection. This result was also confirmed by our experiment.[27] Furthermore, the low Reynolds number code predicts a secondary recirculation zone near the corner of the step. While the secondary recirculation region was confirmed in our experiment when there is side-wall injection, it has never been confirmed for the case without injection.[27] However, the phenomenon was observed by both numerical calculation[28] and experiments[29,30] at lower Reynolds numbers (5×10^3 and 2.2×10^4) which are well over the transition Reynolds number (300–2000 based on the step height)[31,32] for similar configurations. It is still inconclusive at this stage whether the secondary recirculation zone exists at a Reynolds number in the order of 10^5 as in our case. The low Reynolds number model predicts longer reattachment lengths in both CH_4-air and H_2-air combustion cases. The first transverse grid line was pushed further away from the wall boundary in the high Reynolds number simulation in order to ensure that it was not inside the viscous sublayer. Numerical results (not shown here) indicate that the high Reynolds number model predicts both lower mixture fraction and mixture fraction gradient in the near-wall region. One should note that the low Reynolds number model employed in this study has a much denser grid arrangement and

Table 2 Reattachment lengths for various test cases

	Cold flow			Cumbustion			
	High Reynolds no. model	Low Reynolds no. model		High Reynolds no. model		Low Reynolds no. model	
Fuel							
Inj. Vel.[a]	None	None	CH_4	CH_4	H_2	H_2	CH_4
0	0.0	0.27	—	—	—	—	—
m/s	7.26	7.33	—	—	—	—	—
0.477	—	—	0.27	—	—	—	0.52
m/s	—	—	7.33	5.14	—	—	6.05
0.155	—	—	—	—	—	0.57	—
m/s	—	—	—	—	5.09	6.33	—

[a]Injection velocity.

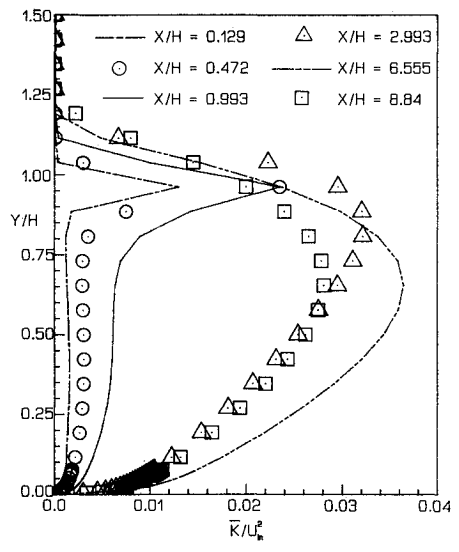

Fig. 4 Normalized turbulence kinetic energy vs Y/H for cold flow simulation without side-wall injection.

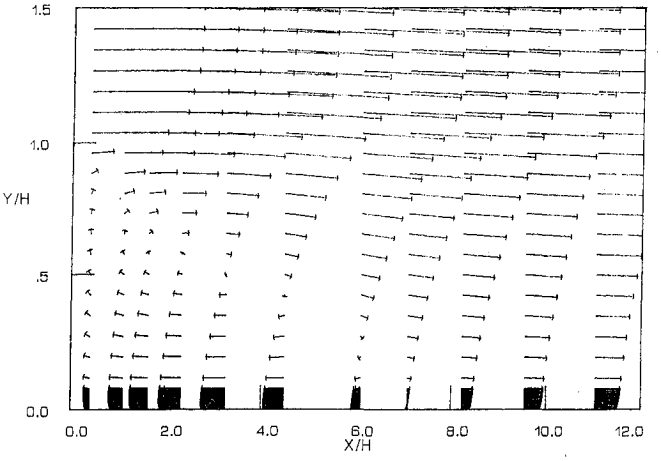

Fig. 5 Velocity vector plot for no-injection case.

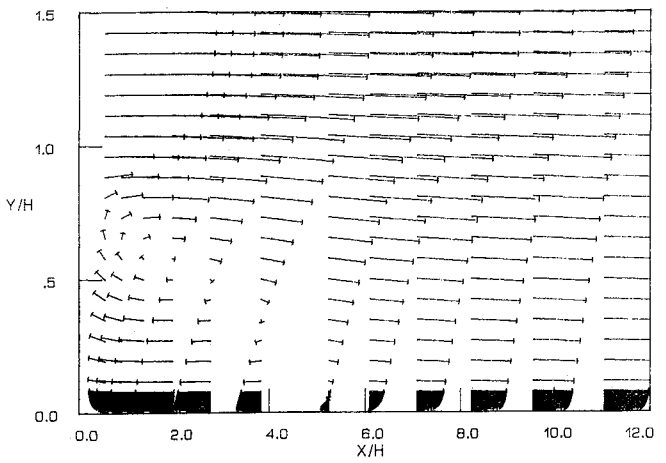

Fig. 6 Velocity vector plot for H_2-air combustion with clipped-Gaussian PDF.

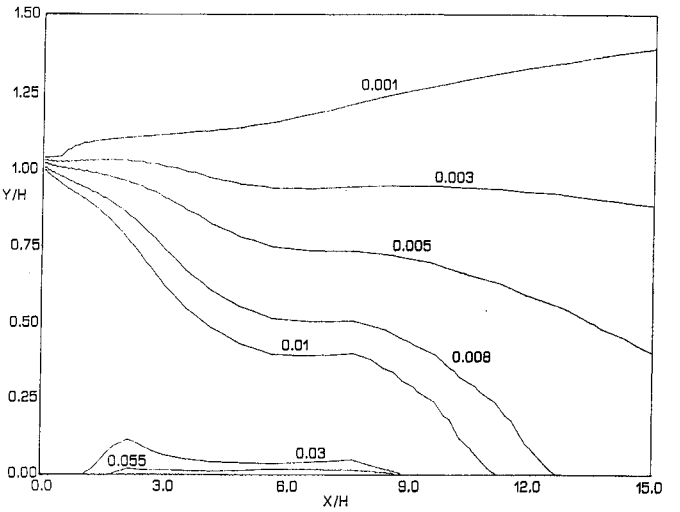

Fig. 8 Contour plot of mixture fraction for CH_4-air combustion assuming no species fluctuations.

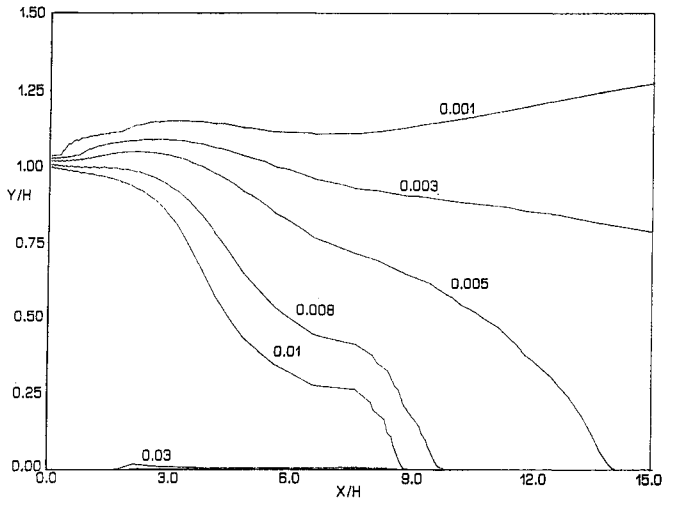

Fig. 7 Contour plot of mixture fraction for cold flow simulation with methane injection.

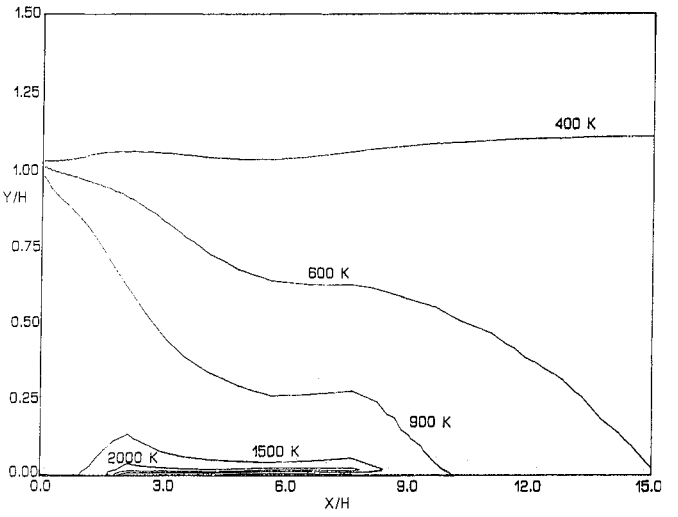

Fig. 9 Contour plot of temperature for CH_4-air combustion assuming no species fluctuations.

includes known turbulence behavior in the near-wall viscous region. Therefore, it is concluded that the results from the high Reynolds number model is prone to be grid dependent due to limitations built in the model itself, and it is especially so for combustion and low injection rate simulations because of higher fuel concentration gradient in the near wall region for those cases.

The two injection velocities shown in Table 2 were determined so that one would have approximately the same amount of heat input to the reactive system. The low Reynolds number model predicts practically the same reattachment lengths for both H_2-air and CH_4-air combustion simulations, whereas the injection velocity of H_2 is 3.2 times higher than that of CH_4. The insensitivity of the reattachment length to the injection velocity is also reflected in the cold flow simulation. De Groot[27] observed the same insensitivity in his cold flow experiments, and Richardson[23] indicated a higher degree of sensitivity in his numerical calculations. It is most likely that the reattachment length is not so sensitive to the injection velocities in the range with which the calculations are concerned. The heat addition to the system acts to shorten the primary reattachment length and elongate the secondary reattachment length, and the amount of heat input is the main factor that determines the size of the recirculation zone behind the step. The reason is that, for approximately the same mean pressure fields, a reactive flow system with lower density experiences a higher adverse acceleration than a nonreactive flow system does.

Figures 5 and 6 are velocity vector plots of cold flow simulation without injection and H_2-air combustion with a clipped-Gaussian PDF model. The big recirculating bubbles can be clearly identified from the plots. The secondary recirculation zones are not shown here. The reactive flow has not only a smaller primary recirculation region but also a center of the recirculation zone closer to the step such that the shear layer initiating from the lip of the step is shifted downward. Any disturbance that will move the separation bubble upstream is likely to break the entire recirculation zone due to the presence of the step and, hence, probably blow off the flame. The separation bubble is, therefore, more stable in a cold flow than in an exothermic, reactive flow in which the longitudinal instability can be enhanced by heat release. The maximum reversal velocity and the velocity in the near-wall region after the reattachment point are increased due to the heat release from chemical reactions. Figures 7 and 8 are contour plots of mixture fraction of CH_4-air cold flow and combustion simulations without considering the species fluctuations. The mixing process in the reactive flow is suppressed because of lower

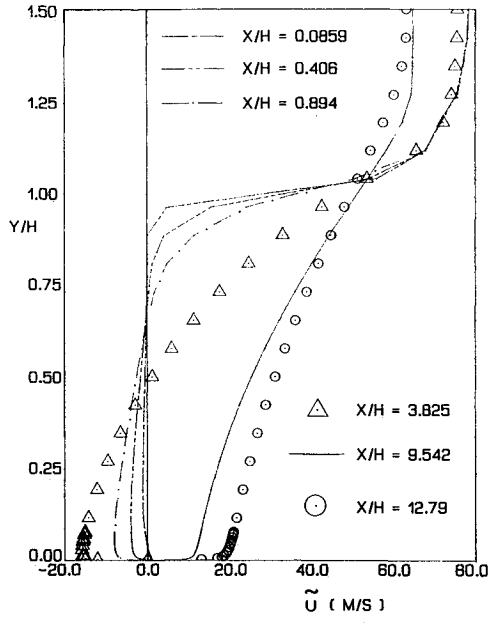

Fig. 10 Velocity profiles at different streamwise locations for cold flow simulation with methane injection.

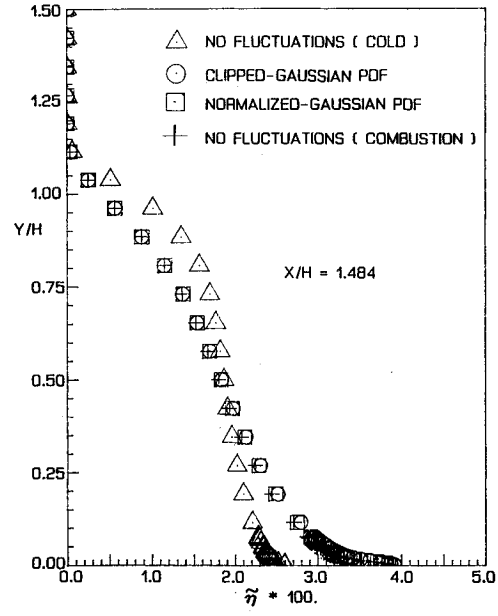

Fig. 12 Mixture fraction profiles for various test cases with injection of methane.

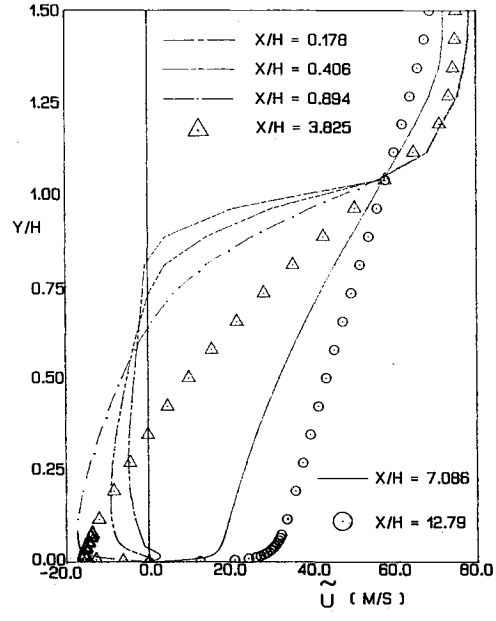

Fig. 11 Velocity profiles at different streamwise locations for CH_4-air combustion with normalized-Gaussian PDF.

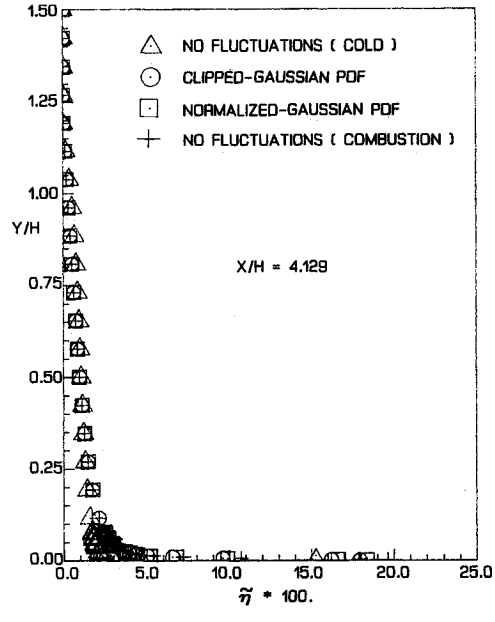

Fig. 13 Mixture fraction profiles for various test cases with injection of methane.

densities, which decreases mass transport and a shorter, downward-shifted shear layer which reduces entrainment of fresh air into the recirculation zone. The weaker mixing in a reactive flow, thus, results in a much higher wall mixture fraction value compared with that of a pure mixing flow. Figure 9 is a temperature contour plot of the CH_4-air combustion case without species fluctuations, which is the same combustion simulation producting Fig. 8. High temperature contours (above 1500 K) concentrate in the neighborhood of the porous plate and the temperatures in the shear layer range from approximately 800 K to the stoichiometric temperature, which is about 2200 K in a contour (not shown) closer to the wall than that of 2000 K shown, of the CH_4-air system.

The symbols and lines in the following figures are to differentiate profiles at different axial locations or combustion models. They all represent numerical results. Figure 10 shows the development of the streamwise velocity along the chamber for the cold flow simulation with CH_4 injection. The profile at $x/H = 0.08587$ shows a small region of positive velocity very close to the wall indicating a countering recirculation zone at the lower left corner of the chamber. As one moves away from the step, the positive velocity in the upper portion of the recirculation zone is gradually increased by momentum transferred from the core region of the flow, and the negative velocity in the lower portion of the recirculation zone approaches its maximum and decreases as one proceeds toward the primary reattachment point. The flow-field relaxes into a channel type of flow after the reattachment point as dictated by the boundary conditions. Figure 11 shows the development of the streamwise velocity along the chamber for CH_4-air combustion case with a normalized-Gaussian PDF model. A countering recirculation region is again observed, and both the

size and the strength are bigger than the one in cold-flow simulation. The velocity deficit between the core region and the retarded and redeveloping region is smoothed out faster than that in the cold-flow simulations because of the heat release and smaller densities, a secondary effect, in the reacting region.

Figure 12 is a combined plot of mixture fraction from various simulated cases at $x/H = 1.484$, which is a station between the inlet step and the fuel bed. A suppression of mixing (less air entrained into the recirculation zone) is clearly observed, which results in a leaner mixture in the upper portion and a richer mixture in the lower portion of the recirculation zone. Figure 13 is a combined plot of mixture fraction at $x/H = 4.129$, which is a station within the fuel port. The same phenomenon observed in Fig. 12 appears, and both the wall mixture fraction value and the gradient are higher in combustion cases. Figure 14 shows combined plots of mixture fraction at $x/H = 10.24$, which is well after the reattachment point. At this station, the mixture fraction profiles of combustion cases gradually catch up the profile of the cold-flow simulation because fuel restrained in the lower part of the recirculation zone is released and diffused into the originally leaner mixture. For all of the combustion simulations, a stoichiometric line is observed initiating from a position slightly ahead of the fuel port, going away from the wall and eventually closing itself back down at a position slightly behind the fuel port. The covariance values are constantly monitored and corrected if necessary in order to ensure that the solution stays within the limit of the statistical models. This study found that the covariance solution satisfies both Eq. (8) and the statistical model applied everywhere except at the vincinity of the reattachment point where corrections are necessary in order to bring the solution back into realizability of the PDF model employed. A possible explanation is that the isotropic turbu-

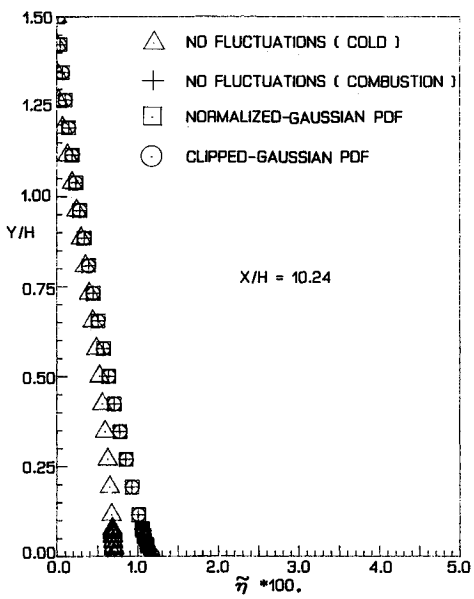

Fig. 14 Mixture fraction profiles for various test cases with injection of methane.

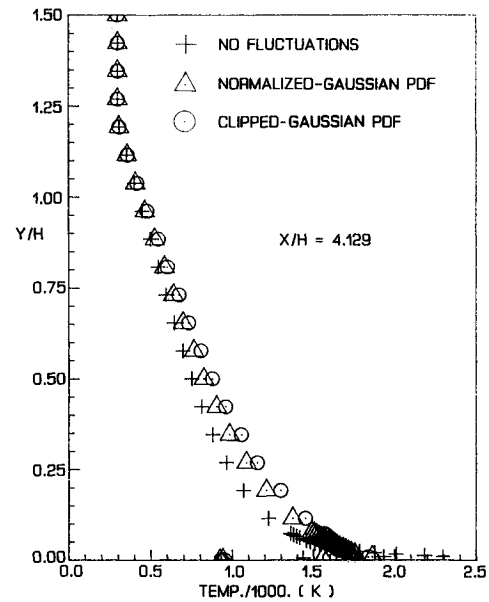

Fig. 16 Temperature profiles for various test cases with injection of methane.

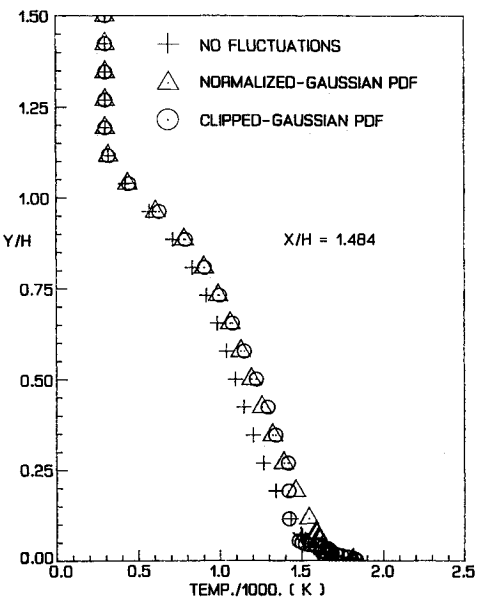

Fig. 15 Temperature profiles for various test cases with injection of methane.

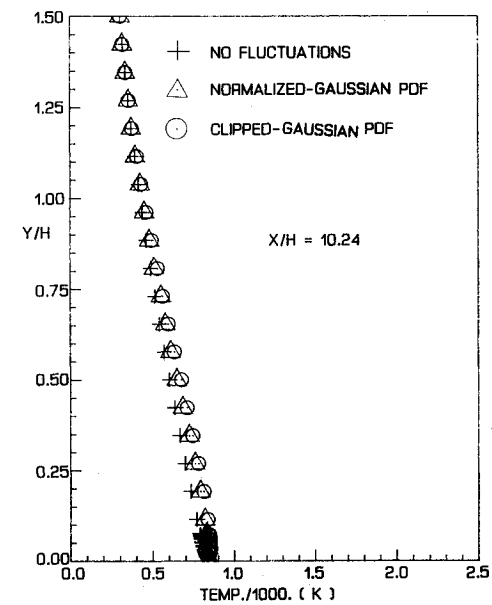

Fig. 17 Temperature profiles for various test cases with injection of methane.

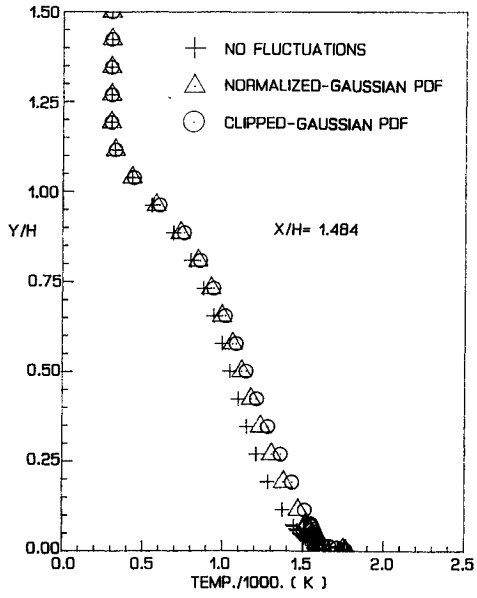

Fig. 18 Temperature profiles for various test cases with injection of hydrogen.

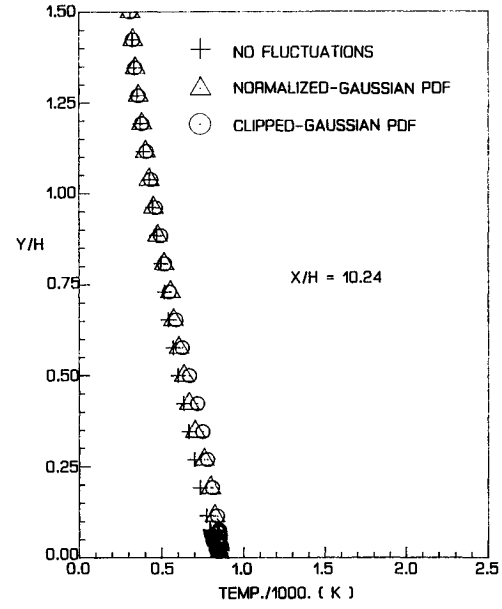

Fig. 20 Temperature profiles for various test cases with injection of hydrogen.

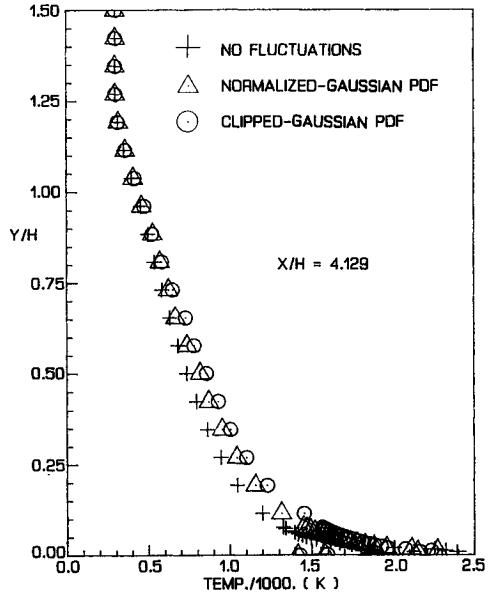

Fig. 19 Temperature profiles for various test cases with injection of hydrogen.

lence assumption, among others, is seriously violated in that region.

Figure 15 shows combined temperature profiles resulting from three combustion models at $x/H = 1.484$ for CH_4-air combustion. The mixture is fuel lean at this station, and temperatures from simulations with species fluctuations taken into account are higher than the ones without considering species fluctuations because of a higher mass transfer rate accompanied by species fluctuations. The difference maximizes at a region slightly above the wall and decreases both towards the wall because fluctuations are diminishing with presence of the wall and away from the wall because the mean mixture fractions are small there. Figure 16 shows combined temperature profiles at $x/H = 4.129$. The mixture is fuel rich on the wall and gets leaner away from the fuel bed at this station. Temperatures from simulations considering species fluctuations are higher than those of simulation without species fluctuations except in the vincinity of the stoichiometric line where the reverse is true due to higher heat transfer rates to the surrounding fluid for simulations with species fluctuations. Temperatures from the normalized-Gaussian PDF model are smaller than those from the clipped-Gaussian PDF model because a clipped-Gaussian PDF allows larger fluctuations (hence larger heat transfer rates) in a flow. At the station $x/H = 10.24$, all of the three temperature profiles almost coincide with each other because the mixture is lean, and the turbulent intensity is low. Figures 18–20, show the same types of behavior for H_2-air combustion cases. The reactive systems eventually relax into an identical thermal system for both H_2-air and CH_4-air cases because the amount of heat input is the same and the fuel injection rates are small compared with the total mass flow rate of the system. The temperature profiles being similar and no large temperature differences resulting from various combustion models suggest that the effect of species fluctuations is small in this investigation.

Conclusion

The turbulent combustion flowfields behind a backward-facing step were studied, and numerical results indicate that the reattachment length is shortened by heat addition into the system and that the amount of heat release is the primary factor in determining the size of the recirculation zone. The newly developed low Reynolds number model predicts longer reattachment lengths than the conventional high Reynolds number model does in combustion simulations. No significant differences (except the temperatures in the vincinity of the stoichiometric line) in the temperature and mixture fraction profiles of the combustion simulations using different combustion models suggest that the species fluctuations effect is small for this flowfield. However, the results obtained by taking into account the species fluctuations are believed to be more realistic than those obtained by neglecting the fluctuations. The mixing process is suppressed by the heat addition to the system. Finally, the conventional high Reynolds number model (boundary conditions) is considered inadequate for reacting flows with wall boundary conditions of the type discussed here.

The use of the present model helps better resolve the near wall region where high temperature and concentration gradi-

ents exist and affect the overall development of the flowfield. Other similar models, e.g., those mentioned in the introduction section or the Reynolds-stress closure model with low Reynolds number approximation near a wall, would also be more suitable for the type of combustion simulation considered here. Although no comparisons are shown between different theoretical models, the current model is certainly superior to any higher-order closure model from an economic point of view and is better than other low Reynolds number models from a physical standpoint.

References

[1]Jones, W. P., and Launder, B. E., "The Prediction of Laminarization With a Two-Equation Model of Turbulence," *International Journal of Heat and Mass Transfer,* Vol. 15, 1972, pp. 301–314.

[2]Launder, B. E., Reece, G. J., and Rodi, W., "Progress in The Development of a Reynolds-Stress Turbulence Closure," *Journal of Fluid Mechanics,* Vol. 68, Pt. 3, 1975, pp. 537–566.

[3]Rodi, W., "Progress in Turbulence Modeling for Incompressible Flows," AIAA Paper 81-0045, 1981.

[4]Launder, B. E., and Spalding, D. B., *Mathematical Models of Turbulence,* Academic, New York, 1972.

[5]Chieng, C. C., and Launder, B. E., "On the Calculation of Turbulent Heat Transport Downstream From an Abrupt Pipe Expansion," *Numerical Heat Transfer,* Vol. 3, 1980, pp. 189–207.

[6]Lam, C. K. G., and Bremhorst, K. A., "Modified Form of the k-ϵ Model for Predicting Wall Turbulence," *Journal of Fluids Engineering,* Vol. 103, 1981, pp. 456–460.

[7]Chien, K. Y., "Predictions of Channel and Boundary-Layer Flows With a Low-Reynolds-Number Turbulence Model," *AIAA Journal,* Vol. 20, 1982, pp. 33–38.

[8]Gorski, J. J., "A New Near-Wall Formulation for the k-ϵ Equations of Turbulence," AIAA Paper 86-0556, 1986.

[9]Bilger, R. W., "Turbulent Jet Diffusion Flames," *Progress in Energy and Combustion Science,* Vol. 1, 1976, pp. 87–109.

[10]Kent, J. H., and Bilger, R. W., "The Prediction of Turbulent Diffusion Flame Fields and Nitric Oxide Formation," Dept. of Mechanical Engineering, The University of Sydney, Sydney, Australia, Kolling Rept. No. 349.

[11]Janicka, J., and Kollmann, W., "A Two-Variable Formalism for the Treatment of Chemical Reactions in Turbulent H_2-Air Diffusion Flames," *Seventeenth Symposium (International) on Combustion,* 1979, pp. 421–430.

[12]Spalding, D. B., "Mixing and Chemical Reaction in Steady Confined Turbulent Flows," *Thirteenth Symposium (International) on Combustion,* The Combustion Institute, Pittsburgh, PA, 1971, pp. 649–657.

[13]Peters, N., and Kee, R. J., "The Computation of Stretched Laminar Methane-Air Diffusion Flames Using a Reduced Four-Step Mechanism," *Combustion and Flame,* Vol. 68, 1987, pp. 17–29.

[14]Drummond, J. P., "Numerical Study of a Ramjet Dump Combustor Flowfield," *AIAA Journal,* Vol. 23, 1985, pp. 604–611.

[15]Rogers, R. C., and Chinitz, W., "Using a Global Hydrogen-Air Combustion Model in Turbulent Reacting Flow Calculation," *AIAA Journal,* Vol. 21, 1983, pp. 586–592.

[16]Ballal, D. R., and Chen, T. H., "Turbulence-Combustion Interaction in Practical Combustion Systems," AIAA Paper 86-1607, 1986.

[17]Spalding, D. B., "Concentration Fluctuation in a Round Turbulent Free Jet," *Chemical Engineering Science,* Vol. 26, 1971, pp. 95–107.

[18]Richardson, J., de Groot, W. A., Jagoda, J. I., Walterick, R. E., Hubbartt, J. E., and Strahle, W. C., "SFRJ Simulator Results: Experiment and Analysis in Cold Flow," *Journal of Propulsion and Power,* Vol. 1, 1985, pp. 488–493.

[19]Jones, W. P., "Models for Turbulent Flows With Variable Density and Combustion," *Prediction Methods for Turbulent Flows,* Hemisphere, Washington, DC, 1980, pp. 379–421.

[20]Strahle, W. C., "Velocity-Pressure Gradient Correlation in Reactive Turbulent Flows," *Combustion Science and Technology,* Vol. 23, 1983, pp. 289–305.

[21]Bilger, R. W., "Turbulent Flows With Nonpremixed Reactants," *Topics in Applied Physics: Turbulent Reacting Flows,* Springer-Verlag, Berlin, 1980, pp. 65–113.

[22]Gordon, S., and McBride, B. J., "Computer Program for Calculation of Complex Chemical Equilibrium Compositions, Rocket Performance, Incident and Reflected Shocks, and Chapman-Jouguet Detonations," Report SP-273, NASA Lewis Research Center, OH, 1971.

[23]Richardson, J., "Analysis of Sudden Expansion Flow in a Two-Dimensional Duct With and Without Side-Wall Injection," Ph.D. Thesis, Georgia Institute of Technology, Atlanta, GA, 1984.

[24]Patel, V. C., Rodi, W., and Scheuerer, G., "Turbulence Models for Near-Wall and Low Reynolds Number Flows: A Review," *AIAA Journal,* Vol. 23, 1985, pp. 1308–1319.

[25]Patankar, S. V., *Numerical Heat Transfer and Fluid Flow,* McGraw-Hill, New York, 1981, pp. 79–120.

[26]Khalil, E. E., *Modeling of Furnaces and Combustors,* Abacus, Cambridge, MA, 1982, pp. 52–72.

[27]de Groot, W. A., "Laser Doppler Diagnostics of the Flow Behind a Backward Facing Step," Ph.D. Thesis, Georgia Institute of Technology, Atlanta, GA, 1985.

[28]Ghoniem, A. F., and Sethian, J. A., "Effect of Reynolds Number on the Structure of Recirculating Flow," *AIAA Journal,* Vol. 25, 1987, pp. 168–171.

[29]Moss, W. D., Baker, S., and Bradbury, L. J. S., "Measurements of Mean Velocity and Reynolds Stresses in Some Regions of Recirculating Flow," *Turbulent Shear Flow I,* Springer-Verlag, New York, 1979, pp. 198–207.

[30]Pitz, R. W., and Daily, J. W., "Combustion in a Turbulent Mixing Layer Formed as a Rearward-Facing Step," *AIAA Journal,* Vol. 21, 1983, pp. 1565–1570.

[31]Durst, F., and Tropea, C., "Flow Over Two-Dimensional Backward-Facing Steps," *Structure of Complex Turbulent Shear Flows,* Springer-Verlag, New York, 1983, pp. 41–52.

[32]Denham, M. K., and Patrick, M. A., "Laminar Flow Over a Downstream Facing Step in a Two-Dimensional Flow Channel," *Transactions of the Institute for Chemical Engineering,* Vol. 52, 1974, pp. 361–367.